Geophys. Res. Lett., **28**, 2393–2396 (2001)

Comparison of Saharan dust aerosol optical depths retrieved using aircraft mounted pyranometers and 2-channel AVHRR algorithms

J.M. Haywood,[1] P.N. Francis,[1] I. Geogdzhayev,[2] M. Mishchenko,[3] and R. Frey[4]

Abstract. The 0.55 μm optical depth of the Saharan dust aerosol plume is determined from C-130 pyranometer data for two different days and the results compared to those from a 2-channel Advanced Very High Resolution Radiometer (AVHRR) retrieval algorithm. When the time difference between the C-130 and AVHRR overpasses is small, the geographic distribution of the aerosol optical depths are similar and differ by less than +/- 0.1 despite the different refractive indices, size distributions and atmospheric profiles implicit in each method. The pyranometer derived optical depth at 0.55 μm exceeds a value of 1 on one of the days, which exceeds the cloud threshold used in many satellite retrieval algorithms with implications for the accuracy of satellite derived aerosol optical depths. The difficulties in making extensive geographical comparisons between satellite and aircraft measurements owing to the differential speed of the observing platforms are also highlighted.

1. Introduction

Saharan dust has received considerable attention because it provides the strongest aerosol signature in satellite retrievals of the aerosol optical depth and perturbation to the clear sky radiation budget over oceanic regions [e.g. *Haywood et al*., 1999, 2001]. While satellite retrievals of aerosol optical depth continue to improve, considerable uncertainty remains in the absolute accuracy of the retrieval algorithms. For example, the single channel AVHRR retrieval algorithm gives optical depths that are typically a factor of 2 less than those using dual wavelength algorithms [*Higurashi and Nakajima*, 1999]. Additionally, while inherent uncertainties in the retrieval algorithms may cancel to some extent in monthly means, *Mishchenko et al.* [2000] suggest that significant uncertainties exist in instantaneous AVHRR derived aerosol optical depth.

This study provides a 'blind' inter-comparison between aerosol optical depths derived from measurements made by the Met Office C-130 and from a 2-channel AVHRR retrieval algorithm for two Saharan dust storms. Sections 2 and 3 describe the derivation of aerosol optical depths from the C-130 and AVHRR measurements. The aerosol optical depths and Ångström coefficients are compared in sections 4 and 5 followed by a discussion and conclusions in section 6.

[1]Met Office, Bracknell, UK.
[2]Columbia University/NASA GISS, NY, USA.
[3]NASA Goddard Institute of Space Science, NY, USA.
[4]University of Wisconsin, WI, USA.

2. C-130 Aerosol Optical Depths, τ_{C130}

Full descriptions of the flights on April 27 and May 8, 1999 and the C-130 instrumentation are provided in *Haywood et al.* [2001]. Briefly, the C-130 flew at approximately constant altitude (22,000-24,000ft) and longitude (18°W) over the dust plume on transit Tenerife-Ascension Island and return. A clear-dome broad band radiometer (BBR) measured the 0.3-3.0 μm upward irradiance. On May 8, the C-130 performed limited aerosol sampling using Particle Measurement Systems (PMS) probes to determine the size distribution and a Particle Soot Absorption Photometer (PSAP) and nephelometer to determine the single scattering albedo.

The direct radiative effect is estimated as the difference between the irradiance modelled using a 4-stream version of the radiative transfer code of *Edwards and Slingo* [1996] excluding aerosols from the calculations, and the measured irradiance. The model surface reflectance is a combination of the broad-band parameterization of *Glew et al*. [2001] and the parameterization detailed in *Thomas and Stamnes* [1999]. Dashed lines in Figure 1 show the modelled 0.3-3.0 μm upward irradiance when aerosols are excluded from the calculations. There is only slight variation in the modelled upward irradiance with latitude due to competing effects of solar zenith angle, θ, and surface reflectance (range 55.7 Wm^{-2} for θ=6° to 54.2 Wm^{-2} for θ=46°). Solid lines show the 0.3-3.0 μm upward irradiances measured by the BBR. The difference between the modelled and measured irradiances is the instantaneous clear-sky direct solar radiative effect which is as strong as –60 Wm^{-2} in Figure 1b. The estimated error in the modelled and measured irradiances is ±5 Wm^{-2} [*Haywood et al*., 2001] therefore the 'positive' radiative effect seen to the North of 19°N (i.e. when the modelled irradiance exceeds the measured irradiance) is explained by the errors in the measurements and modelling.

To derive τ_{C130} a method similar to that of *Haywood et al*. [2001] is used. Aerosol optical properties are determined by Mie scattering theory assuming the refractive indices of dust-like aerosol from *WCP* [1986] using the measured in-situ size distributions from the PMS probes. Only limited sampling of the aerosol confined to the region marked 'profiles' on Figure 1a was possible due to aircraft fuel constraints. The aerosol size distribution obtained from 10 minutes of straight and level runs at an altitude of 8000 ft is shown in Figure 2. Analysis of relative humidity from drop-sondes reveals that the relative humidity does not exceed 50 % in the aerosol layer so the effects of relative humidity on the size distribution are neglected [*Haywood et al*., 2001]. At 0.55 μm the single scattering albedo, w_0=0.87, asymmetry factor, g=0.73 and specific extinction coefficient, k_e=0.68 m^2g^{-1}. w_0 is in good agreement with that derived from the PSAP and nephelometer

and the wavelength dependence of k_e is in encouraging agreement with the optical depth measured at Sal, Cape Verde Islands [*Haywood et al*., 2001]. The optical properties are similar to those from the desert dust model of *Hess et al*. [1998] who used 4-log normal distribution components and calculated w_0=0.86, g=0.73 and k_e=0.68 m^2g^{-1} for a wavelength of 0.55 µm. This good agreement is due to the observed and modelled size distributions being in good agreement (Figure 2). No size distributions are available for April 27.

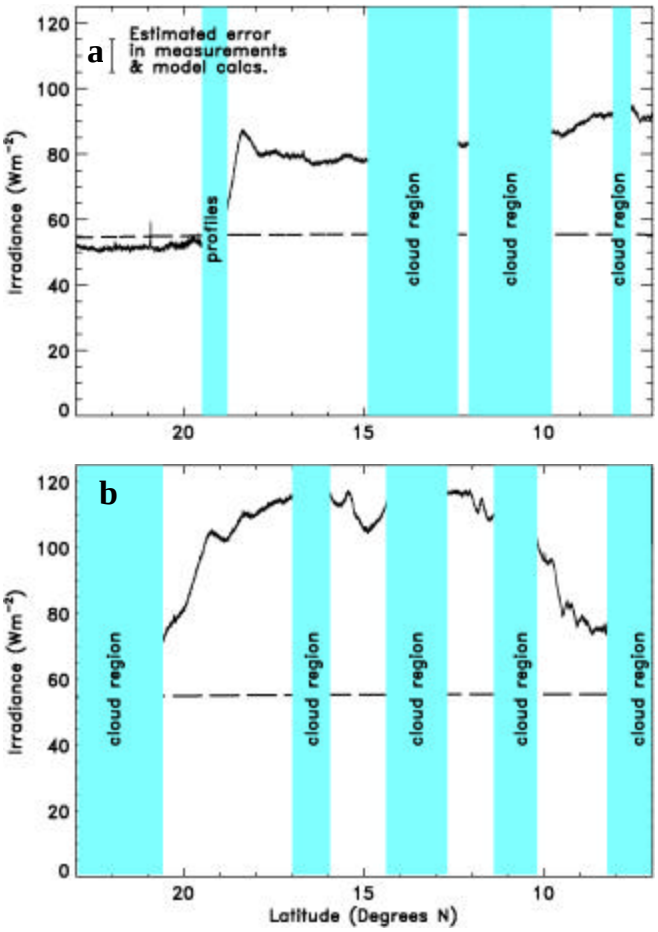

Figure 1. Solid lines represent the measured 0.3-3.0µm irradiances. Dashed lines represent the modelled irradiance in the absence of aerosols. Regions of cloud are excluded, as are areas where the C-130 was performing profiles into the aerosol layer. a) May 8, b) April 27.

To calculate τ_{C130} for May 8, a layer of mineral dust (constant number density) with the optical parameters derived from the measured size distribution shown in Figure 2 is inserted between 650-875 hPa which back-trajectory analyses, tephigrams from drop-sondes, and in-situ sampling suggest is the likely position of the dust layer [*Haywood et al*., 2001]. The aerosol number density is then adjusted until the modelled 0.3-3.0 µm upward irradiance agrees with the observations shown in Figure 1b, and τ_{C130} at 0.55 µm calculated. The most practical procedure for performing these calculations is to make a look-up table that determines the irradiance for a range of solar zenith angles and aerosol burdens, and bi-linear interpolation is used to estimate τ_{C130}.

As in other modelling studies, the variation of the upward irradiance with solar zenith angle is stronger for high optical depths than for low optical depths due to the shape of the aerosol phase function [e.g. *Haywood and Shine*, 1997; *Boucher et al*., 1999]. The sensitivity of the TOA clear-sky direct radiative effect is calculated to be approximately -39 Wm^{-2}/τ to –55 Wm^{-2}/τ for $\theta=0^o$, and –36 Wm^{-2}/τ to –76 Wm^{-2}/τ for $\theta=46^o$. Application of k_e=0.68 m^2g^{-1} determines a normalised clear-sky radiative effect of –53 Wg^{-1} to –112 Wg^{-1}.

3. AVHRR Aerosol Optical Depths, τ_{AVHRR}

τ_{AVHRR} is determined from Local Area Coverage radiance data (resolution 1x1km) for a longitude of 18°W (the track of the C-130) for April 27 and May 8, 1999. Because of the differential velocity of the C-130 and the AVHRR satellite we consider τ_{AVHRR} and τ_{C130} co-located in space, but not in time. A stringent cloud-screening algorithm that relies on a combination of reflectance and brightness temperature thresholds, and spatial inhomogeneity criteria [*M^{c}Clain*, 1989] is applied. Subsequently, the 2-channel τ_{AVHRR} retrieval algorithm described in full by *Mishchenko et al.* [2000] is applied to the radiances. In brief, this algorithm uses look-up tables that store theoretical channel 1 (0.65 µm) and channel 2 (0.85 µm) reflectances derived using a radiation code based on that of *Hansen and Travis* [1974] for all viewing geometries and aerosol and atmospheric parameters. By best fitting the measured and theoretical radiances, τ_{AVHRR} and the Ångström coefficient at 0.55 µm are derived.

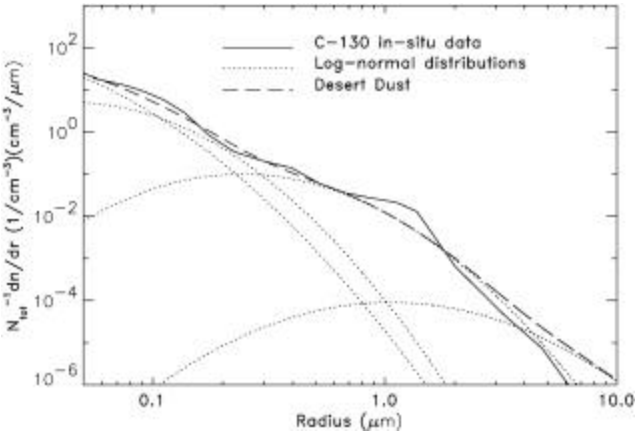

Figure 2. The size distribution of the aerosol measured by the PCASP-100X on the C-130 aircraft (solid line), together with the four log-normal components (dotted lines) that make up the desert dust model (dashed line) from Hess *et al*. (1998).

4. Comparison of τ_{C130} and τ_{AVHRR}

A comparison of τ_{C130} and τ_{AVHRR} at 0.55 µm is shown in Figure 3. Dots represent τ_{C130} with selected points marked by circles and estimates of the error (±5 Wm^{-2}) which translates to

an uncertainty of ±0.1 (assuming a RMS error of ±7 Wm^{-2}). τ_{AVHRR} is shown by the triangles.

For May 8, τ_{C130} is not calculated in the 'profiles' section in Figure 1 because the C-130 was operating within the aerosol layer. The strict criterion that no τ_{AVHRR} was retrieved if the viewing angle was within 40° of specular reflection [*Mishchenko et al.*, 2000] was relaxed; a less stringent 30° criterion was applied. Nevertheless, sun-glint truncated τ_{AVHRR} retrievals to northwards of 16°N. τ_{AVHRR} was smoothed using a running mean of 10 LAC pixels to aid visual comparison. τ_{C130} and τ_{AVHRR} show an almost step change at a latitude of 19°N.

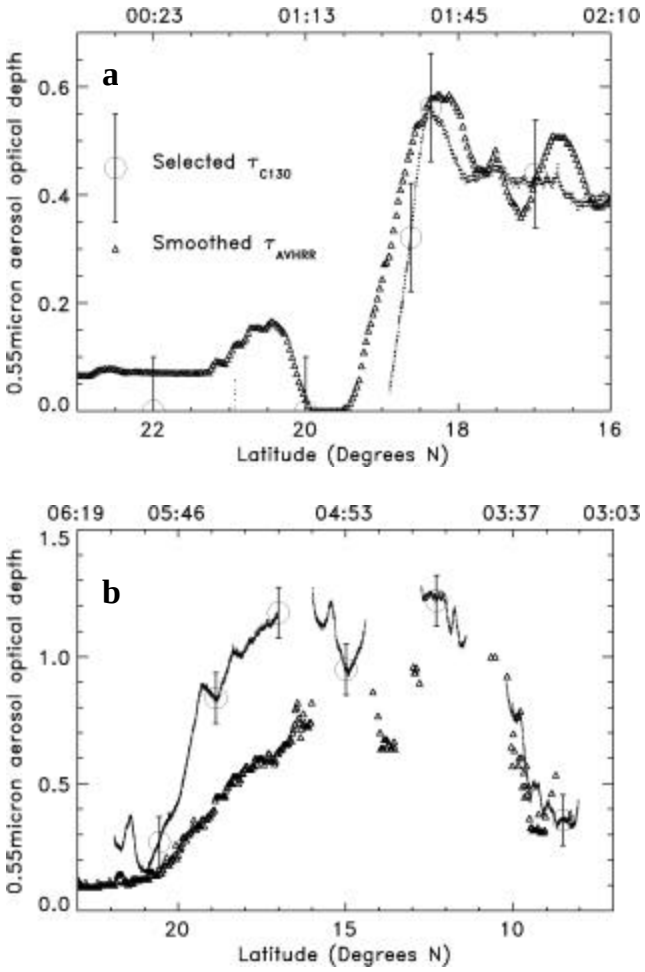

Figure 3. Comparison of τ_{C130} and τ_{AVHRR}. Dots show τ_{C130} with selected points highlighted by circles and error bars. τ_{AVHRR} are shown by the triangles. a) May 8, b) April 27. The time between the C-130 and AVHRR overpass is shown at the top of each plot.

Visual observations from the C-130 suggested an abrupt clearance of the aerosol plume and that northward of approximately 19°N that τ_{C130} was low. Both τ_{C130} and τ_{AVHRR} show the lowest values northward of 19.5°N, τ_{C130} reaching zero where model irradiances are larger than the measurements (Figure 1a). Southward of 19.5°N, both τ_{C130} and τ_{AVHRR} show the same feature of a peak between 18-18.5°N. Southward of 18.5°, the agreement between τ_{C130} and τ_{AVHRR} is within the ±0.1 estimated error in τ_{C130}. It is difficult to assess the effects of the lack of temporal co-location when comparing τ_{C130} and τ_{AVHRR} shown in Figure 3a. For May 8, the C-130 overpasses at the extreme latitudes of 16°N and 23°N were at 14:04GMT and 16:02GMT respectively with corresponding AVHRR overpasses at 16:12GMT and 16:14GMT. Thus, τ_{AVHRR} and τ_{C130} data are not temporally co-located at any of the latitudes shown in Figure 3a. In the transition region between the low and high aerosol optical depth region (18.5°N-19.5°N) τ_{AVHRR} is outside τ_{C130} ±0.1. However, at 19°N, 1½ hours elapse between the overpass of the C-130 and AVHRR. The mean components of wind-speed in the layer 650-750mb were 4.4 ms^{-1} N (stdev=0.5 ms^{-1}), 13.1 ms^{-1} E (stdev=0.4 ms^{-1}). Thus in 1½ hours, the dust may be advected 24 km or 0.22° to the north. If this is accounted for, τ_{AVHRR} is within τ_{C130} ±0.1. Obviously this analysis is idealized as it assumes that the aerosol optical depth is homogeneous in the zonal direction, and ignores differential advection at different altitudes. Investigating the dynamical evolution of the dust plume is beyond the scope of this study.

For April 27, τ_{C130} is calculated assuming the same size distribution as in Figure 2, a necessary assumption because no in-situ sampling of the dust layer was performed. Regions where cloud was detected in the AVHRR retrievals and in the C-130 retrievals are excluded. No smoothing to τ_{AVHRR} was necessary for this case. The results show significant differences northwards of 10°N, but good agreement between approximately 10°N and 8°N. The C-130 overpasses at the extreme latitudes of 23°N and 7°N were at 10:14GMT and 13:30GMT respectively with corresponding AVHRR overpasses at 16:37GMT and 16:32GMT. It is difficult to assess the effects of advection. Wind-speeds data from drop-sondes was available for latitudes of 22.9°N, 14.7°N, and 10.6°N revealing that the aerosol plume is subject to differential advection across the plume. For example, at 875 hPa, the northward component of the wind speed is 12 ms^{-1} at 22.9°N, while at 10.6°N, the southward component of the wind speed is 5 ms^{-1}. These complexities demonstrate the problems in comparing aircraft derived aerosol optical depths over a large region with those from satellites. However, τ_{C130} and τ_{AVHRR} are in significantly better agreement to the south of the operating region where the wind-speeds and time between the observations are smallest.

5. Comparison of $Å_{C130}$ and $Å_{C130}$

The Ångström coefficient at 0.55 μm, *Å*, is defined by *Mishchenko et al.* [2000] as $Å = d[\ln s_{ext}]/d[\ln l]|_{l=0.55}$, where s_{ext} is the extinction coefficient at a wavelength λ. *Å* is a measure of the rate of change of the extinction coefficient with wavelength, and gives an indication of the size of the particle distribution. $Å_{C130}$ calculated at 0.55 μm for the size distribution shown in Figure 2 is 0.27. This is in good agreement with $Å_{AVHRR}$ for the latitudinal range 16°N-19°N, which reveals a mean $Å_{AVHRR}$ for May 8 of 0.31 (stdev 0.13). For April 27, the mean over the latitude range 7°N-23°N is 0.51 (stdev 0.16) suggesting that the size distribution contains proportionally more small particles than May 8. Thus the

assumption that the size distribution and optical parameters are identical to those of May 8 may not be valid.

6. Discussion and Conclusions

For May 8, the results from the 'blind' inter-comparison when τ_{C130} and τ_{AVHRR} are derived independently show similar spatial distributions and magnitudes with differences in aerosol optical depths of less than ± 0.1. The results for April 27 are not as robust as for May 8 owing to the lack of in-situ aerosol sampling. However, τ_{AVHRR} is generally within $\tau_{C130} \pm 0.1$ when the time between C-130 and AVHRR overpasses is less than approximately 4 hours. This agreement between τ_{C130} and τ_{AVHRR} is encouraging, as the derivation methods are quite different. Radiance derived optical depths may be subject to uncertainties due to the effects of non-sphericity influencing the aerosol scattering phase function [*Mishchenko et al.*, 1995]. Irradiance derived optical depths are not as sensitive to viewing geometry as the aerosol scattering phase function is averaged over the up-scattered hemisphere. The good agreement between $Å_{C130}$ and $Å_{AVHRR}$ on May 8 suggests the satellite retrieval algorithm is able to determine the wavelength dependence of the extinction coefficient and the size distribution of the particles to a reasonable accuracy.

Sensitivity tests indicate that τ_{C130} is sensitive to the imaginary part of the refractive index (m). Application of wavelength independent im of 0.002 and 0.010 in place of *WCP* [1986] leads τ_{C130} a factor of 0.72 and 1.20 of those derived here. These ims are within the range reported in previous studies of Saharan dust aerosol [e.g. *Sokolik et al.* 1993; *Ignatov* 1995], although they produce widely different single scattering albedos ($\omega_{o,\lambda=0.55\mu m}$=0.95 for im=0.002, and $\omega_{o,\lambda=0.55\mu m}$=0.83 for im=0.010).

Finally, τ_{C130} exceeds 1 on April 27, which is the threshold above which aerosol is assigned as cloud in some aerosol retrieval algorithms. Thus instantaneous aerosol retrieval algorithms may misclassify optically thick Saharan dust aerosol as cloud, with implications for monthly mean aerosol optical depths.

Acknowledgments. I. Geogdzhayev and M. Mishchenko's contribution was funded by the NASA GACP project. The crew of the C-130 are thanked for their efforts. John Edwards is thanked for developing the radiation code. Manfred Wendisch and an anonymous reviewer are thanked for reviewing the manuscript.

References

Boucher, O., S.E. Schwartz, T.P. Ackerman, T.L. Anderson, B. Bergstrom, B. Bonnel, P. Chýlek, A. Dahlback, Y. Fouquart, Q. Fu, R.N. Halthore, J.M. Haywood, T. Iversen, S. Kato, S. Kinne, A. Kirkevåg, K.R. Knapp, A. Lacis, I. Laszlo, M.I. Mishchenko, S. Nemesure, V. Ramaswamy, D.L. Roberts, P. Russell, M.E. Schlesinger, G.L. Stephens, R. Wagener, M. Wang, J. Wong, and F. Yang, Intercomparison of models representing direct shortwave radiative forcing by sulfate aerosols. *J. Geophys. Res*., 103, 16979-16998, 1998.

Edwards, J.M., and A. Slingo, Studies with a flexible new radiation code. I: Choosing a configuration for a large scale model, *Q. J. R. Meteorol. Soc*., 122, 689-720, 1996.

Glew, M.D., P. Hignett, and J.P. Taylor, Aircraft measurements of sea surface albedo. *J. Atmos. Sci*.,, in press, 2001.

Hansen, J.E., and L.D. Travis, Light scattering in planetary atmospheres, Space Sci. Rev., 16, 527-610, 1974.

Haywood, J.M., P.N. Francis, M.D. Glew, and J.P. Taylor, The optical properties and direct radiative effect of Saharan dust: A case study of two Saharan dust outbreaks using aircraft data. *J. Geophys. Res.*, in press, 2001.

Haywood, J.M., Ramaswamy, V., Soden, B.J., Tropospheric aerosol climate forcing in clear-sky satellite observations over the oceans. *Science* 283, 1299-1303, 1999.

Haywood, J.M. and K.P. Shine, Multi-spectral calculations of the direct radiative forcing of tropospheric sulphate and soot aerosols using a column model, *Q. J. R. Meteorol. Soc*., *123*, 1907-1930, 1997.

Hess, M., P. Koepke, and I. Schult, Optical properties of aerosols and clouds: the software package OPAC, *BAMS*, 1998.

Higurashi, A., and T. Nakajima, Development of a two-channel aerosol retrieval algorithm on a global scale using NOAA AVHRR, *J. Atmos. Sci*., 56, 924-941, 1999.

Ignatov, A.M., L.L. Stowe, S.M. Sakerin, and G.K. Korotaev, Validation of the NOAA/NESDIS satellite aerosol product over the North Atlantic in 1989. *J. Geophys. Res*., 100, 5123-5132.

M^{c}Clain, E.P, Global sea surface temperatures and cloud clearing for aerosol optical depth estimates, *Int J. Remote Sens*., 10, 763-769, 1989.

Mishchenko, M. I., A. A. Lacis, B. E. Carlson, and L. D. Travis, Nonsphericity of dust-like tropospheric aerosols: implications for aerosol remote sensing and climate modeling, *Geophys. Res. Lett*. 22, 1077-1080, 1995.

Mishchenko, M. I., I. V. Geogdzhayev, B. Cairns, W. B. Rossow, and A. Lacis, Aerosol retrievals over the ocean by use of channels 1 and 2 AVHRR data: sensitivity analysis and preliminary results. *Applied Optics*, 38, 7325-7341, 2000.

Sokolik, I., Andronova, A., and T.C. Johnson, Complex refractive index of atmospheric dust aerosols, *Atmos Environ*., 27A, 2495-2502, 1993.

Thomas, G.E., and K. Stamnes, *Radiative Transfer in the Atmosphere and Ocean*, Cambridge University Press, 1999

WCP (World Climate Program), *A Preliminary Cloudless Standard Atmosphere for Radiation Computation*, World Meteorological Organisation, Geneva, 1986.

J.M. Haywood, and P.N. Francis, Met Office, Y46 Building, DERA, Fanborough, Hants, GU14 0LX, UK. (e-mail: jim.haywood@metoffice.com; pete.francis@metoffice.com)

I. Geogdzhayev, and M. Mishchenko, NASA, Goddard Institute of Space Science, 2880 Broadway, New York, NY 10025, USA. (e-mail: igor@giss.nasa.gov; crmim@stokes.giss.nasa.gov)

R.A. Frey, Space Science and Engineering Center, 1225 West Dayton St., Madison, WI 53706, USA. (e-mail: richard.frey@ssec.wisc.edu).

(Received: November 14, 2000; revised: March 26, 2001; accepted: April 2, 2001)